THE ASTROPHYSICAL JOURNAL, 445:269–279, 1995 May 20

MAGNETIC FIELDS AROUND BOK GLOBULES: CCD POLARIMETRY OF CB 4

BRIAN D. KANE AND DAN P. CLEMENS
Astronomy Department, Boston University, 725 Commonwealth Avenue, Boston, MA 02215
ROBERT W. LEACH
Astronomy Department, College of Sciences, San Diego State University, San Diego, CA 92182-0334
AND
RICHARD BARVAINIS
Haystack Observatory, NEROC, Route 40, Westford, MA 01886
Received 1994 August 22; accepted 1994 November 11

ABSTRACT

The small Bok globule CB 4 was probed using a CCD imaging polarimeter in order to create a detailed map of the magnetic field associated with this cloud. Stars as faint as 17th mag at V band were measured polarimetrically with uncertainties less than 1%. Sky transmission variations were minimized via a system of synchronous polaroid rotation and bidirectional charge shifting. In all, 80 stars behind the periphery of the globule were accurately analyzed polarimetrically. The large-scale (1–2 pc) magnetic field direction around CB 4 was found to be very uniform (P.A. = $63\overset{\circ}{.}3 \pm 1\overset{\circ}{.}1$). Double-Gaussian fitting of the polarization position angle histogram gave a dispersion of 10° about the primary field direction. Possible field-line compression was found inward of ~0.2 pc from the cloud center. No appreciable twisting of field lines was found. By plotting stellar separations against differences of polarization position angles, CB 4 was found to have a magnetic field decorrelation length of ~0.1 pc, similar to the size of the visually opaque core, but much smaller than the size of the bright optical rim or CO half-power contour of ~0.5 pc. The magnetic field decorrelation length may be related to a characteristic transient clumping size, or perhaps even to clumps of a more permanent nature.

Subject headings: dust, extinction — ISM: individual (CB 4) — ISM: magnetic fields — polarization — techniques: polarimetric

1. INTRODUCTION

Isolated, small Bok globules are the simplest subset of molecular clouds which can form stars (Clemens & Barvainis 1988, hereafter CB; Yun & Clemens 1990). Such clouds are ideal physical laboratories for the investigation of the relationship between structure, kinematics, and embedded magnetic fields during various stages of star formation.

IRAS observations of warm dust in Bok globules have been effective in identifying nearly all the young stellar objects (YSOs) embedded in these nearby clouds (Yun 1993). Many globules, however, show no signs of embedded YSOs. These quiescent clouds form an even simpler subset of molecular clouds, a subset which can provide the cleanest laboratory for investigations of the mostly unstudied, early evolutionary stages which precede core collapse and subsequent star formation, including how ambient magnetic fields interact with clumpy gas and dust cores.

Gas kinematics and density structures in these quiescent globule cores are determined via millimeter and submillimeter spectroscopic observations of trace molecules such as CO and its isotopes (e.g., Martin & Barrett 1978; Leung, Kutner, & Mead 1982; Dickman & Clemens 1983, hereafter DC). These observations can also be used to determine whether rotation is an important evolutionary factor in quiescent globules (Aquilla & Goldsmith 1986).

In contrast, determining the properties of the ambient magnetic field has been much more difficult. While magnetic fields are generally thought to give support against gravitational collapse (Shu, Adams, & Lizano 1987, and references therein), mediate disk formation and accretion in YSOs (e.g., Mouschovias & Paleologou 1980; Königl 1989), and help direct YSO winds and outflows (Blandford & Payne 1982), the strengths of the magnetic fields are very difficult to measure in molecular clouds (Goodman et al. 1989). Nevertheless, it is relatively easy to measure the directional pattern of the magnetic field, via polarimetry, in the near environs of dark clouds and cores (e.g., Vrba et al. 1986). Light from unpolarized background stars is thought to become linearly polarized via processes which magnetically align dust grains.

Efforts to date have shown a variety of magnetic field patterns in Bok globules and dark clouds (Vrba et al. 1986; Hodapp 1987; Klebe & Jones 1990; Myers & Goodman 1991, hereafter MG). Field patterns surrounding many globules (e.g., B5, Joshi et al. 1985; B118, B133, B361, Klebe & Jones 1990; B335, Vrba et al. 1986 and Hodapp 1987; and L810, Hodapp 1987) are predominantly uniform, but show some evidence of cometary extensions. Some globules and other dark clouds exhibit field patterns whose uniform component is parallel to the Galactic plane (B118, B133, B361, Klebe & Jones 1990; and CB 4, this paper), while others show field patterns which are apparently decoupled from the surrounding Galactic field (L810, Hodapp 1987; and L1506, L1755, Perseus, Goodman et al. 1990). Patterns of dark-cloud magnetic field directions and measurements of the rms dispersions of those directions have been utilized by MG to build a classification scheme consisting of five magnetic field pattern classes.

Optical stellar polarimetry generally has been performed in single-aperture mode, resulting in several times 10^1 stars being polarimetrically measured per cloud. These numbers are not nearly high enough to allow unique characterizations of the magnetic field patterns for those clouds (see Vrba et al. 1986; Hodapp 1987). In order to obtain an adequate stellar sample of

$\sim 10^2$ stars from a typical apparent magnitude distribution near Bok globules, it is necessary to measure with accuracy the polarized emission from stars as faint as 17–18 mag in the V band (Clemens & Leach 1987). The smallest of these globules are typically no more than 4′ in diameter; the magnetic field directional maps so produced will be very detailed.

Magnetic fields typically impress only weak linear polarization signatures on starlight ($\sim 1\%$–5%), requiring polarimetric uncertainty at the subpercent level. Such accuracy coupled with an adequate star sample size has not been previously achieved with routine single-aperture polarimetry. These requirements can be met with CCD imaging techniques, provided that sky variation effects are minimized. In this paper, we present the results of the first detailed investigation of a Bok globule magnetic field using a CCD-based polarimeter.

The field pattern around CB 4, one among a new sample of starless small Bok globules, is revealed and examined in this paper. CB 4 is an excellent target of study both because it is far from the Galactic plane ($b = -10°$) and because it has a relatively well determined distance, 600 pc (DC). It is very well isolated from the effects of star-forming regions, and it has been spectroscopically studied in CO and its isotopes (DC; Kane & Clemens 1995). From its lack of detectable NH_3 or HC_3N emission, it can be surmised that CB 4 does not contain an extremely dense ($n > 10^4$ cm^{-3}) core (Kane, Clemens, & Myers 1994). CB 4 thus best represents the paradigm of a simple, quiescent, starless molecular cloud.

In the following sections, details of the technical requirements for the CCD polarimeter are described, followed by the new results for the magnetic field associated with CB 4, and a discussion of its dynamical state.

2. INSTRUMENTATION AND OBSERVATIONS

Accurate polarimetry for 100–200 stars in the very close environments of small Bok globules, whose field sizes are $\sim 8' \times 8'$, was identified as a long-term goal of our investigation. Meeting this goal required removal of short-term sky variations at a level not routinely achieved using CCDs with fixed-angle polaroids (see Zaritsky et al. 1987).

The CCDPOL instrument, designed to meet the sensitivity, stability, and areal coverage requirements, consisted of an 800 × 800 TI CCD, camera electronics capable of bidirectional charge shifting, a computer-controlled rotating polaroid (HN38 plus quarter-wave plate) section, and a fast mechanical shutter (Clemens & Leach 1987).

In order to obtain polarimetric images, the CCD was initially flushed, the polaroid rotated to a fiducial position angle, and the shutter closed. The shutter was next opened for a short integration period (less than 1–10 s), forming an image of the sky on the CCD, and then closed. The polaroid position angle was rotated, generally by 90°, and the CCD photoelectrons shifted down (the normal readout direction) by 15–20 rows (many times the point-spread function [PSF] size of the stellar images). The shutter was again opened and closed to form an image on the CCD, this time through the polaroid at its new orientation angle. Once the shutter was closed, the polaroid was rotated back to its original position, and the CCD photoelectrons shifted up (away from the readout) by the same 15–20 rows. This cycle was repeated some 20–100 times to build up a doubled image, which contains all the information necessary to form either a Stokes U- or Stokes Q-value for each star that appears doubled on the image. Because of the moderately fast sky chopping achieved by this system, short-term (minutes) sky variations are frozen, enabling high polarimetric accuracy.

Verification and characterization of the performance of the instrument was handled in two ways: (1) via observations of polarimetric standard stars, and (2) via analysis of the repeatability of globule field star polarimetric values.

Moderately faint polarimetric standard stars were chosen from the lists of Mathewson & Ford (1970) and Hall (1958), and one of these stars was also observed using the single-pixel polarimeter MINIPOL (Clemens & Tapia 1990). Since the standards were much brighter than the normal globule field stars (6–9th mag vs. 12–17th mag), a 4.8% neutral density filter was added to the optical path to diminish the standards to $\sim$9–12th mag at the CCD.

Observations of polarimetric standard stars and of the fields containing CB 4 were performed during late December of 1986 using the University of Arizona 1.55 m telescope on Mount Bigelow, north of Tucson, Arizona. The TI 800 × 800 CCD format was on-chip binned to 400 × 400 pixels, each pixel viewing $\sim 0\farcs62$ of sky on a side. Four fields were initially imaged to cover a region of $\sim 8' \times 8'$ surrounding CB 4 (fields a, b, c, and d; see Fig. 1). Twelve, 2 minute duration, V-band

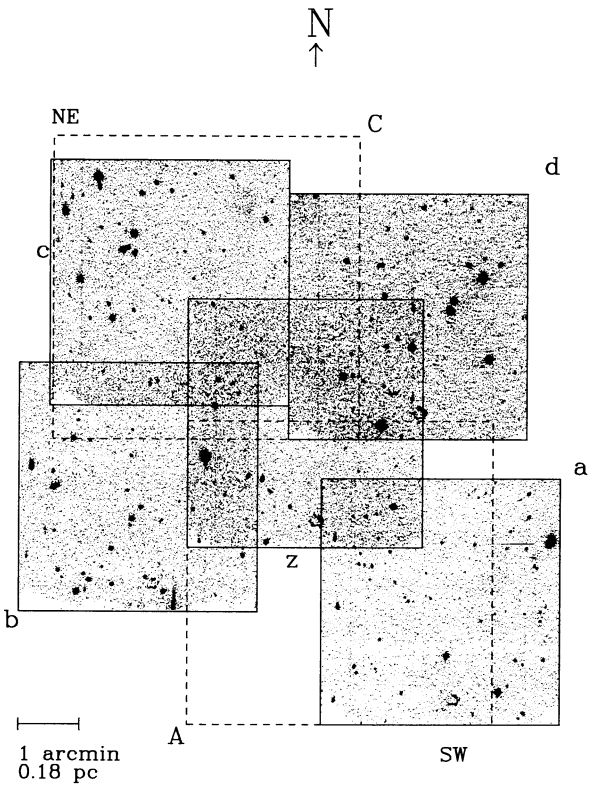

FIG. 1.—V-band mosaic of the region around CB 4 ($\alpha_{2000} = 0^h39^m05\overset{s}{.}1$, $\delta_{2000} = +52°52'06''$). Images made in the central frame z, centered on the optically opaque region defining CB 4, were used for photometric calibrations, and contained no polarimetric information. Twelve 2 minute polarimetric exposures of 4′ × 4′ fields, in each of frames a–d, were made with $\sim 0\farcs6$ pixel^{-1} sampling. Eight 5 minute polarimetric exposures of 5′ × 5′ fields, of frames A and C, were made with a slightly different optical configuration giving $\sim 0\farcs74$ pixel^{-1} sampling. Since no photometric exposures were taken of frames A and C, their field-of-view outlines are marked on the mosaic with dashed lines.

polarimetric images were collected for each of the four fields, six for the creation of Stokes U-values and six for Stokes Q. Two other fields (A and C) were reobserved during the same run with a slightly larger pixel size (0".74) and using longer integrations (eight images of 5 minute duration each, four in U and four in Q). The mean PSF FWHM size was $\sim$3 pixels ($\sim$2").

3. DATA REDUCTION AND CALIBRATION

IRAF[1] routines were used to bias-correct, find stars, and perform aperture photometry of all stellar images above 5 σ of the background noise level, for 10 different aperture sizes ranging from 1".5 to 6" in radius. Because the stellar images for each U or Q pair were formed onto the same pixel(s) on the CCD, no flat-fielding was applied to the polarimetric images. Each frame was inspected for hot pixels, streaks, and other defects, as well as stellar blends. After rejecting star pairs contaminated by any of these effects, an average of $\sim$35–40 stellar pairs per frame per field were deemed suitable for polarimetric analysis.

Custom software was used to collect the photometry for the stellar pairs and to match stars across frames and fields. Accurate polarimetric data for each detected star pair was matched for $\sim$70% of the frames in which the stars appeared. Most failures in matching occurred for star pairs near the edges of the images, when one or both stars in the pair drifted off the edge during the time between successive frame exposures. Other matching failures were attributable to CCD chip defects, described above.

Repeatability of the polarization values was examined via analysis of the multiple Stokes U and Q images collected for each field (generally between eight and 20 independent frames). Stokes parameters were extracted independently for each star (for all 10 apertures photometered) from each frame and combined to establish mean values and dispersions for each star. As shown in Figure 2, the resulting polarization uncertainties (propagation of the U and Q mean errors from the multiple measurements) are subpercent in the V band for many stars down to almost 18th mag. The final polarization data for each star was obtained by choosing the minimum uncertainty in the percentage polarization from the set of data obtained through the 10 different apertures.

A slightly different procedure was used to image the polarimetric standard stars. After each standard was imaged through the first polaroid position angle, the shutter was closed, the photoelectrons shifted downward, but the polaroid was only rotated 45° between successive openings of the shutter. *Four* stellar images were formed via repetition of this method, yielding a complete set of Stokes U and Q parameters for each CCD frame. The foursomes were similarly photometered, but the photometric data were separated into U pairs and Q pairs, to facilitate processing with the same custom software used to analyze the field star polarimetry. Similarly, the best of 10 different apertures was chosen according to the minimum polarimetric uncertainty, and the apparent linear polarization position angles for each standard star were regressed against their standard equatorial values, to obtain an instrumental offset angle.

Table 1 presents the standard stars, their standard values,

[1] IRAF is distributed by National Optical Astronomy Observatories, which are operated by the Association of Universities for Research in Astronomy, Inc., under contract with the National Science Foundation.

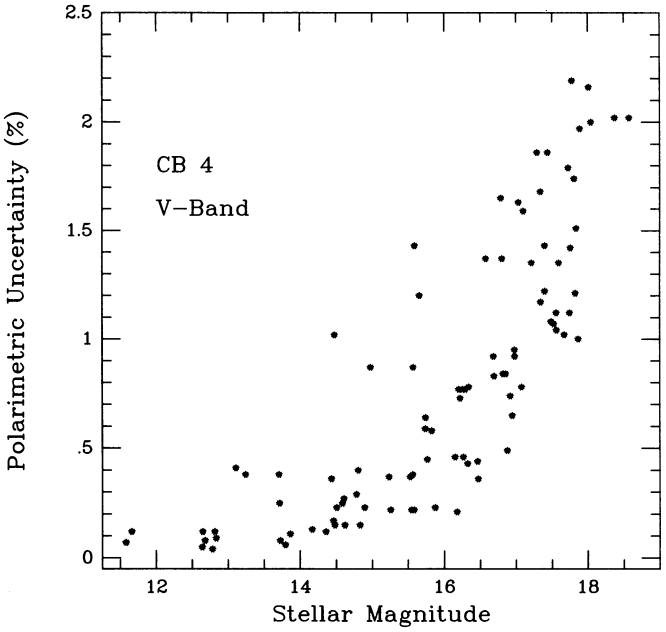

FIG. 2.—Plot of the polarimetric uncertainty vs. the V-band magnitude of stars imaged around CB 4. The polarimetric uncertainty was derived from the dispersion of Stokes U- and Q-values obtained from 12 different images of each field.

and the values measured using the CCDPOL instrument. All position angles with positive values have been measured east from north. Figure 3 shows the regression of the results of observations of the 10 standards in the equatorial versus instrument position angle plane. A further comparison of the Stokes U and Q in the equatorial and rotated instrumental systems established the polarization signature inherently added by the instrument. By choosing the U- and Q-values from the best apertures for each standard star and accumulating total $U_{EQU} - U_{CCDPOL}$ and $Q_{EQU} - Q_{CCDPOL}$ distributions, the instrumental polarization was determined to be 0.68% $\pm$ 0.13% along P.A. = 87°.

To obtain a polarization position angle map of the field stars surrounding CB 4, coordinates were first established from identification of *Hubble Space Telescope* (*HST*) Guide Star Catalog (GSC) stars found in the images. Frame-to-frame overlap offsets were determined, and each star assigned equatorial coordinates, epoch 2000.0. The stellar polarimetric values were corrected for the instrumental terms, and for their Ricean distribution (Barvainis 1984). Stars with final polarimetric position angle uncertainties greater than 15° were culled.

The resulting polarimetric database, summarized in Table 2, consists of 80 stars whose polarimetric position angle uncertainties are less than 15°. Column (1) lists the sequence of stars numbered by increasing right ascension, while columns (2) and (3) list the epoch 2000.0 equatorial coordinates of right ascension and declination for each star. Column (4) lists approximate V-band magnitudes (uncertainties $\sim$0.3 mag). Columns (5)–(8) list polarization percentages and position angles, and their uncertainties. All position angles have been measured east from north. Finally, column (9) lists notes relevant to frame positioning, exposure times, and data averaging. The polarization percentages and position angles for these stars are presented in Figure 4.

TABLE 1

POLARIMETRIC STANDARD STAR DATA

Star (1)	R.A. (J2000) (2)	Decl. (J2000) (3)	m_V (mag) (4)	P_{EQU} (5)	χ_{EQU} (6)	P_{CCDPOL} (7)	P.A.$_{CCDPOL}$ (8)	References (9)
S1. HD 832.....	$00^h10^m12^s$	5°54'00"	9.4	0.23%	66°	0.30%(0.15%)	−51°(14°)	1
S2. HD 3644	00 36 37	−4 16 02	9.0	0.41	123	1.51 (0.24)	−53 (5)	1
S3. HD 236954.....	02 10 03	58 56 14	9.4	6.39	113	6.42 (0.18)	−20 (1)	2
S4. HD 17747.....	02 48 41	26 24 31	8.5	0.89	140	1.26 (0.13)	8 (3)	1
S5. HD 25330.....	03 59 02	09 51 33	5.7	1.52	134	2.17 (0.36)	3 (5)	1
S6. HD 29557.....	04 36 12	−24 46 00	8.6	1.10	51	2.94 (0.63)	−47 (6)	1
S7. HD 245310.....	05 33 24	21 09 21	9.1	3.91	146	1.21 (0.46)	18 (11)	2
S8. HD 43384.....	06 14 00	23 45 00	6.3	2.75	171	2.68 (0.09)	39 (1)	1, 2
S9. HD 58624.....	07 24 12	16 13 00	9.0	1.11	27	1.52 (0.36)	−86 (7)	1
S10. HD 94473.....	10 51 36	−26 29 00	7.3	1.00	63	4.71 (1.68)	−42 (10)	1, 3

REFERENCES.—(1) Mathewson & Ford 1970; (2) Hall 1958; (3) Clemens & Tapia 1990.

4. THE MAGNETIC FIELD

4.1. *Morphology of the Uniform Field*

The position angle distributions of most dark clouds show single, distinct local maxima and have dispersions between 10° and 20° (MG). In this section, the distributions of polarizations and position angles for stars behind the periphery of CB 4 are studied, in order to characterize the nature of the magnetic field of this globule.

The histogram of polarization position angles, Figure 5, shows a strong peak around the mean position angle 65°, with a calculated dispersion of 13°. This position angle indicates the preferred regional magnetic field direction, and the narrow width of the peak indicates a largely uniform field. The gas distribution, as traced via CO mapping, exhibits a major axis which lies at a position angle of ~45° (Kane & Clemens 1995), less than 20° away from the mean field direction.

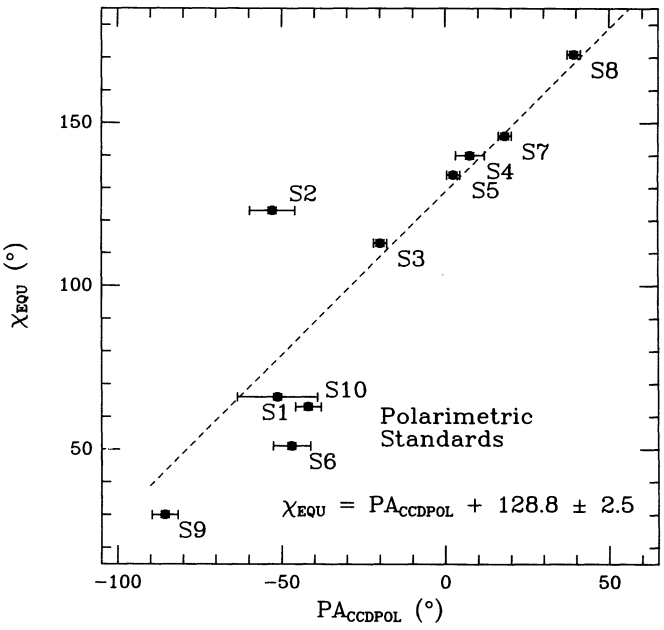

FIG. 3.—Comparison of the raw polarimetric position angles measured by the CCDPOL instrument (P.A.$_{CCDPOL}$) for 10 intermediate-magnitude polarization standard stars vs. their equatorial coordinate standard values (χ_{EQU}). This regression establishes the instrumental offset angle, relative to the equatorial system, and the absolute direction of polaroid rotation.

HD 3901 and HD 3950 are stars near CB 4, both in equatorial coordinates, and in inferred distance from the Sun (~500 pc). These stars have equatorial (measured east with respect to equatorial north) polarization position angles of 78° and 82°, respectively, and polarizations of ~1% (Hall 1958). The position angles are only ~15° from the mean direction seen in Figure 5, and the polarizations are roughly equal to the mean percentage polarization seen around CB 4 (Fig. 8, below). The direction of the Galactic plane (increasing longitude) is 88° relative to equatorial north at the position of CB 4. With a difference angle of only 23°, the local field around CB 4 appears to be moderately coupled to the Galactic field.

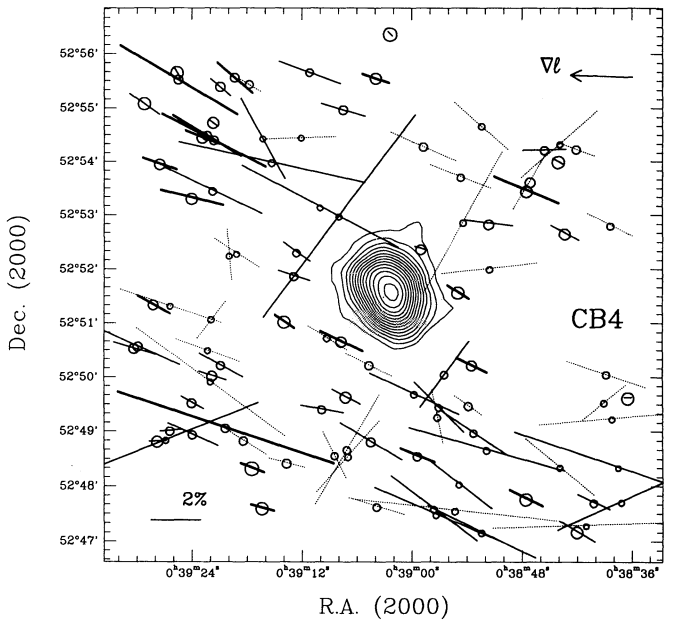

FIG. 4.—Summary of polarization percentages and position angles for 80 stars imaged near the CB 4 globule and having position angle uncertainties less than 15°. Stellar positions are represented by open circles with sizes roughly proportional to magnitudes of apparent brightness. Polarization vector directions parallel the magnetic field direction, while vector lengths represent polarization percentages. Boldface vectors have position angle uncertainties less than 5°, while nonboldface solid vectors have uncertainties between 5° and 10°. Dashed-line vectors represent polarizations with position angle uncertainties greater than 10°. The contours represent velocity-integrated ^{13}CO line emission (Kane & Clemens 1995). A 2%-long key is shown in the lower left, while the gradient of Galactic longitude is shown in the upper right.

TABLE 2

POLARIMETRIC DATA FOR CB 4 FIELD STARS

Star (1)	R.A. (J2000) (2)	Decl. (J2000) (3)	m_V (mag) (4)	P (5)	σ_P (6)	χ (7)	σ_χ (8)	Notes (9)
1.....	00^{h}38^{m}36^s.47	52°49′37″.6	12.64	0.30%	0.05%	88°.2	4°.8	a, m, g 1993
2.....	00 38 37.21	52 47 43.5	17.94	5.49	1.79	116.2	9.3	a
3.....	00 38 37.56	52 48 21.4	18.12	8.68	1.97	69.6	6.5	a
4.....	00 38 38.24	52 49 14.6	18.07	5.30	2.57	95.6	13.9	a
5.....	00 38 38.39	52 52 49.5	16.98	1.89	0.92	61.1	14.0	d
6.....	00 38 39.09	52 49 32.2	17.27	2.15	0.95	132.0	12.7	a
7.....	00 38 40.25	52 47 42.9	16.68	1.39	0.44	63.3	9.1	a
8.....	00 38 41.10	52 47 17.9	18.38	6.75	3.27	92.0	13.9	a
9.....	00 38 42.08	52 47 11.1	13.38	1.66	0.41	57.5	7.1	a
10.....	00 38 42.12	52 54 14.1	16.13	1.50	0.64	67.6	12.2	d
11.....	00 38 43.36	52 52 40.4	13.93	1.26	0.38	59.1	8.6	d
12.....	00 38 43.91	52 54 19.9	17.81	4.01	1.68	135.0	12.0	d
13.....	00 38 43.94	52 48 21.6	18.05	3.39	1.51	47.6	12.8	a
14.....	00 38 44.06	52 54 00.5	13.17	0.49	0.08	55.7	4.6	d
15.....	00 38 45.57	52 54 13.3	16.09	1.63	0.59	92.1	10.4	d
16.....	00 38 47.14	52 53 38.2	14.68	1.73	1.02	152.6	10.7	d
17.....	00 38 47.53	52 53 28.1	13.65	2.85	0.38	64.8	3.8	d
18.....	00 38 47.62	52 47 47.1	13.93	1.52	0.06	61.2	1.1	A, a
19.....	00 38 51.63	52 52 51.2	14.86	1.91	0.36	82.2	5.4	d
20.....	00 38 51.88	52 48 40.6	18.13	6.15	2.16	72.8	10.1	A
21.....	00 38 52.44	52 47 10.3	17.32	4.63	1.63	61.7	10.1	a
22.....	00 38 53.31	52 48 59.2	17.65	3.16	1.07	53.1	9.7	A
23.....	00 38 53.47	52 50 13.3	14.62	1.37	0.12	62.1	2.5	a, A
24.....	00 38 53.87	52 49 28.8	17.06	1.26	0.65	51.8	14.7	A
25.....	00 38 54.88	52 48 03.2	17.69	3.30	1.04	49.4	9.0	a, A
26.....	00 38 54.94	52 51 34.5	13.13	1.07	0.04	55.1	1.1	d, A
27.....	00 38 55.30	52 47 34.2	18.40	7.43	3.74	83.4	14.4	A
28.....	00 38 56.44	52 50 03.4	17.55	3.37	1.22	146.6	10.4	A
29.....	00 38 57.07	52 49 27.1	17.80	2.84	1.00	41.3	10.1	A
30.....	00 38 57.36	52 47 29.8	17.50	5.33	1.43	64.8	7.7	a, A
31.....	00 38 57.62	52 47 36.0	16.99	4.29	1.37	50.2	9.2	a, A
32.....	00 38 59.00	52 52 23.2	15.01	0.52	0.15	71.3	8.3	d
33.....	00 38 59.41	52 48 34.0	15.91	1.49	0.22	66.1	4.2	a, A
34.....	00 38 59.74	52 49 41.6	16.94	3.94	0.74	62.7	5.4	a, A
35.....	00 39 02.39	52 56 22.2	11.58	0.27	0.07	42.4	7.4	m, g 605
36.....	00 39 03.97	52 55 32.5	14.83	1.16	0.15	69.7	3.7	C
37.....	00 39 04.47	52 48 49.2	16.20	2.88	0.77	56.1	7.7	A
38.....	00 39 04.60	52 50 13.4	16.55	2.02	0.83	61.1	11.8	A
39.....	00 39 07.16	52 49 38.1	15.02	1.27	0.40	60.1	9.0	A
40.....	00 39 07.54	52 54 57.8	15.35	1.83	0.37	71.9	5.8	c, C
41.....	00 39 07.65	52 50 40.0	16.89	1.94	0.23	62.1	3.4	A
42.....	00 39 07.95	52 52 59.5	18.57	10.89	2.02	146.4	5.3	C
43.....	00 39 09.20	52 50 43.7	16.82	1.73	0.84	55.3	13.9	b
44.....	00 39 09.80	52 49 24.7	16.26	1.69	0.46	79.2	7.8	b
45.....	00 39 10.03	52 53 09.7	18.01	6.98	2.19	59.4	9.0	c
46.....	00 39 11.20	52 55 39.3	16.65	2.55	0.78	68.0	8.8	c, C
47.....	00 39 12.59	52 52 19.2	16.76	1.34	0.36	51.8	7.7	b, C
48.....	00 39 12.88	52 51 52.7	15.91	1.30	0.38	70.3	8.4	b, C
49.....	00 39 13.91	52 51 01.7	13.17	1.01	0.09	53.2	2.6	b, A
50.....	00 39 15.32	52 53 59.2	18.17	7.53	1.74	76.1	6.6	C
51.....	00 39 16.32	52 54 25.8	18.03	3.95	1.02	25.9	7.4	c, C
52.....	00 39 16.33	52 47 36.5	12.65	0.97	0.12	73.6	3.5	m, g 509
53.....	00 39 17.41	52 48 20.1	11.66	1.03	0.12	66.6	3.3	m, g 853
54.....	00 39 17.77	52 55 25.6	16.88	0.95	0.49	56.5	14.8	C, c
55.....	00 39 18.32	52 48 50.2	15.75	2.11	0.87	55.1	11.8	b
56.....	00 39 19.38	52 55 33.4	16.17	1.97	0.21	46.4	3.1	C, c
57.....	00 39 20.29	52 49 04.2	16.12	9.19	1.20	69.8	3.7	b
58.....	00 39 20.82	52 50 13.2	16.00	2.01	0.45	59.0	6.4	b
59.....	00 39 20.93	52 55 23.0	15.89	1.09	0.23	46.9	6.1	C, c
60.....	00 39 21.65	52 54 23.9	15.62	4.81	0.37	59.9	2.2	c, C
61.....	00 39 21.73	52 54 43.2	14.03	0.47	0.08	50.4	4.8	c, C
62.....	00 39 21.75	52 50 01.6	14.87	1.14	0.27	70.0	6.8	b
63.....	00 39 21.76	52 53 27.6	17.45	4.26	1.35	61.6	9.1	C, c

TABLE 2.—*Continued*

Star (1)	R.A. (J2000) (2)	Decl. (J2000) (3)	m_V (mag) (4)	P (5)	σ_P (6)	χ (7)	σ_χ (8)	Notes (9)
64.....	00 39 21.87	52 51 04.0	17.28	1.88	0.78	145.4	11.9	b
65.....	00 39 22.41	52 54 29.1	16.40	3.28	0.43	56.2	3.8	C, c
66.....	00 39 22.91	52 54 27.3	14.56	1.47	0.23	66.4	4.5	C, c
67.....	00 39 23.89	52 48 56.8	16.00	2.18	0.58	63.3	7.6	b
68.....	00 39 23.97	52 49 31.7	15.45	1.04	0.22	58.5	6.1	b
69.....	00 39 24.04	52 53 19.5	14.66	2.62	0.17	74.5	1.9	C, c
70.....	00 39 25.50	52 55 31.1	16.53	5.60	0.73	56.6	3.7	C
71.....	00 39 25.68	52 55 39.0	13.12	0.55	0.12	28.6	6.3	c, C
72.....	00 39 26.32	52 51 19.1	17.60	3.91	1.86	69.6	13.6	b
73.....	00 39 26.32	52 49 01.0	15.73	0.82	0.22	94.6	7.7	b
74.....	00 39 26.77	52 48 50.9	17.77	7.67	2.63	114.1	9.8	b
75.....	00 39 27.55	52 53 57.6	14.44	1.47	0.13	68.4	2.5	c, C
76.....	00 39 27.71	52 48 49.2	14.08	0.67	0.11	92.7	4.7	b
77.....	00 39 28.18	52 51 20.5	14.89	1.51	0.25	58.5	4.7	b, C
78.....	00 39 29.24	52 55 04.4	14.07	1.50	0.25	51.8	4.8	C
79.....	00 39 29.82	52 50 34.1	15.09	3.59	0.87	63.3	7.0	b
80.....	00 39 30.27	52 50 32.1	14.99	1.74	0.29	71.2	4.8	b

NOTES.—Multiple notes indicate weighted-average data from multiple frames: m—Minipol star data (Clemens & Tapia 1990); g—GSC star (followed by GSC number in table); a—24 minute integration in frame a (see Fig. 1); b—24 minute integration in frame b (see Fig. 1); c—24 minute integration in frame c (see Fig. 1); d—24 minute integration in frame d (see Fig. 1); A—40 minute integration in frame A (see Fig. 1); C—40 minute integration in frame C (see Fig. 1).

The rough alignment of the major axis of the dust in the globule with the projected direction of the magnetic field is seen in the *IRAS* 100 μm co-added opacity image of the region, constructed using the method detailed in Clemens, Yun, & Heyer (1991). Contours of 100 μm opacity are shown in Figure 6, overlaid with the stellar positions and polarimetric data.

Is the dust responsible for the extended far-infrared emission also responsible for the polarization signatures impressed on the background starlight? This question can be answered by inspection of Figure 7, which plots percentage polarization of each star against the corresponding 100 μm optical depth at the position of each star. A straight-line fit with a positive slope would indicate a correlation, but instead the optical depth bears almost no relationship to the degree of polarization. The linear correlation coefficient for all the data is 0.18, corresponding to a 7% chance that the data are correlated. The correlation, if it exists at all, is very weak. Polarization increases at only 0.04% per 10^{-6} unit of 100 μm opacity. Dust which does not strongly emit at far-infrared wavelengths,

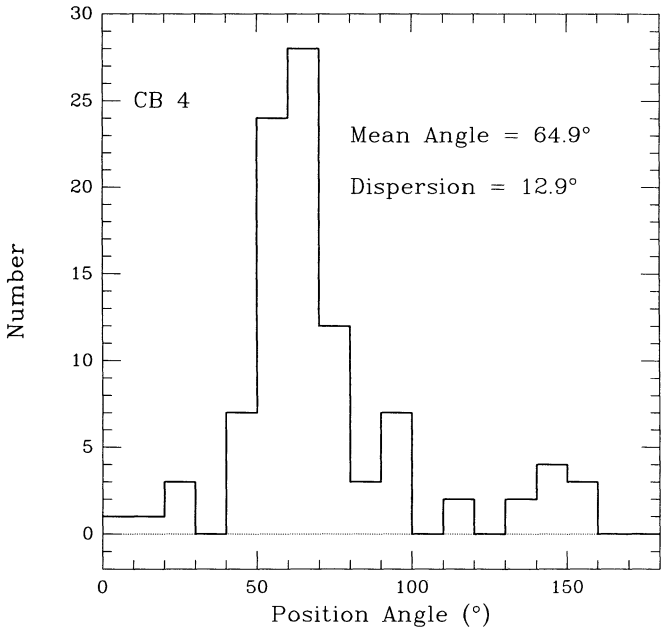

FIG. 5.—Distribution of polarization position angles for stars in the vicinity of CB 4. The strong peak between 60° and 70° is evidence for a uniform magnetic field threading through the globule. The dispersion of 13° is typical of the dark-cloud sample studied by Myers & Goodman (1991).

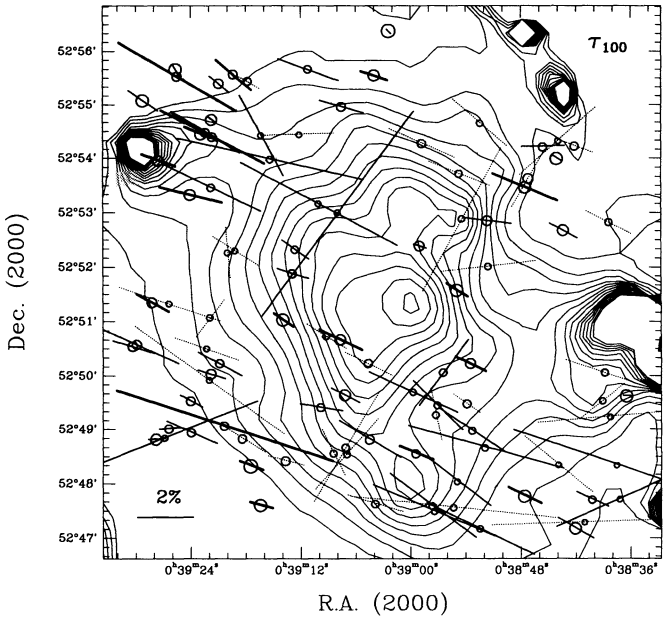

FIG. 6.—Same as Fig. 4, but superimposed upon contours of 100 μm opacity constructed from co-added *IRAS* survey images. The opacity contours range from 1×10^{-6} to 1.4×10^{-5} in steps of 1×10^{-6}.

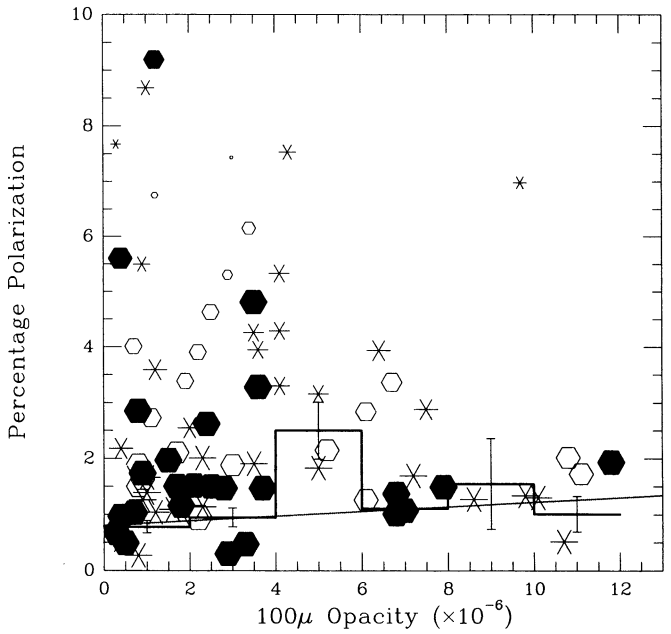

FIG. 7.—Distribution of stellar percentage polarizations with *IRAS* 100 μm opacities at the corresponding stellar positions. Three different symbols are shown: filled hexagons represent stars with polarization position angle uncertainties less than 5°; asterisks for those with uncertainties between 5° and 10°; open hexagons for those with uncertainties between 10° and 15°. The size of each symbol is roughly inversely proportional to the uncertainty in the polarization. The histogram shows the polarization uncertainty weighted means and mean errors, and the dotted line is the weighted linear least-squares fit to all of the data points.

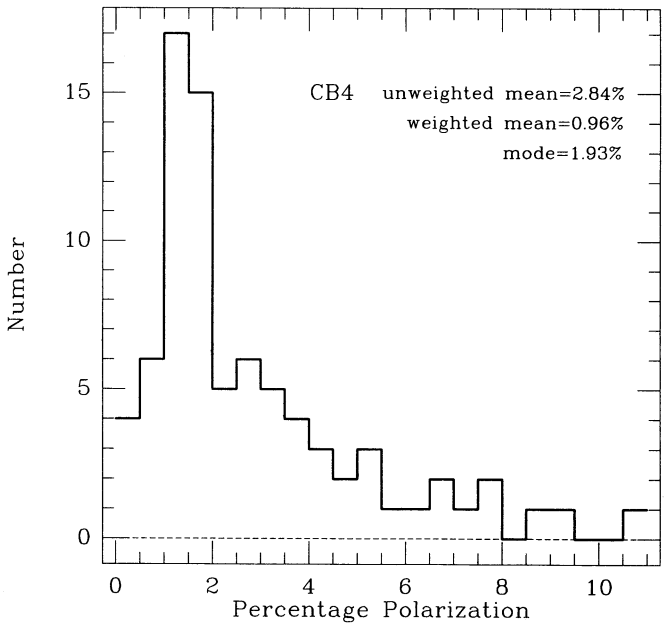

FIG. 8.—Distribution of polarization percentages for stars in the vicinity of CB 4. The mean value around 3% is typical of anisotropic absorption from dust (Jones 1989), and the sharp decline in lower polarization percentages indicates that the stellar polarization sample is only complete down to 1%. Most subpercent polarization values were culled due to their large corresponding position angle uncertainties.

because of size, shape, or composition, is most likely responsible for the linear polarization.

The value of the dispersion of polarization position angles is close to the midpoint of the distribution of dispersion (15°) seen in a sample of 15 dark clouds (MG). However, if *two* Gaussians are fit to the histogram of polarization position angles (Fig. 5), the principle peak occurs at 61°.4 ± 0°.5, and the dispersion is only 10°.0 ± 0°.6. A small secondary peak occurs at 147°.5 ± 1°.5 (~90° from the first), with a dispersion of 7°.9 ± 1°.4. Both the Gaussian-fit dispersion of the primary peak and its error (normalized to the dispersion) are about one-third smaller than the mean dispersion and its error in the MG sample (16°.0 ± 1°.8).

Figure 8 shows the distribution of Ricean-corrected polarization percentages. The Rice factor, $[1 - (\sigma_P^2/P^2)]^{1/2}$, corrects P for its non-Gaussian distribution. The distribution of polarization percentages is clearly sensitivity limited, as evidenced by the steep fall-off below 1%. However, the singly peaked polarization percentage (mean value 2.84% ± 0.25%, inverse rms^2 weighted mean value 0.96% ± 0.07%) indicates a largely uniform magnetic field, as seen for the polarization position angle distribution.

Figures 9*a* and 9*b* show the dependence of mean percentage polarization and mean position angle, respectively, with increasing distance from the center of CB 4. Means were inverse rms^2 weighted, and error bars denote the error of the mean. Taking unweighted means does not appreciably alter the distributions.

Figure 9*a* shows that outside 3′ radius, the mean percentage polarization is generally flat, remaining near 1%, slightly higher than the mean polarization value of 0.5% induced by dust in the local Galactic field (Hall 1958; Mathewson & Ford 1970). From 3′ radius inward, two trends are seen. There is a substantial increase in observed polarization in the 2′–3′ radius bin (about twice the radius of the half-power ^{13}CO contour). Inside 2′ radius, however, the percentage polarization decreases to nearly the background value.

Figure 9*b* also shows a noticeable trend. A linear least-squares fit to the binned position angle data yields an intercept of 53° ± 9° and a slope of 3°.6 ± 2°.3 arcmin^{-1}. The linear correlation coefficient is only 0.68, and thus this trend is as likely due to random sampling as it is due to large-scale field twisting. For a fit to the unbinned data, the linear correlation coefficient is only 0.11, for a trend likelihood of less than 9%.

4.2. *Morphology of the Nonuniform Field*

Typical dispersions in the direction of linear polarization are many times greater than measurement uncertainties and provide evidence of the existence of a nonuniform component to the interstellar magnetic field (MG). The magnitude of the dispersion and the distribution of dispersion with various geometrical parameters (e.g., radius, azimuth, and separation) may yield important information about the nature of the nonuniform field. Magnetic field variations are thought to arise from hydromagnetic waves (MG). In this section, several tests are made of the nature of the nonuniform field. Because of the large number of stars analyzed, it is possible to make such tests for the first time.

4.2.1. *Field Compression*

The possible presence of a compression in the field lines near the gas density peak in the globule can be examined by plotting radial bins (normalized to the mean distance of all stellar positions from the globular center) of the weighted average difference in polarization position angle from the global (all

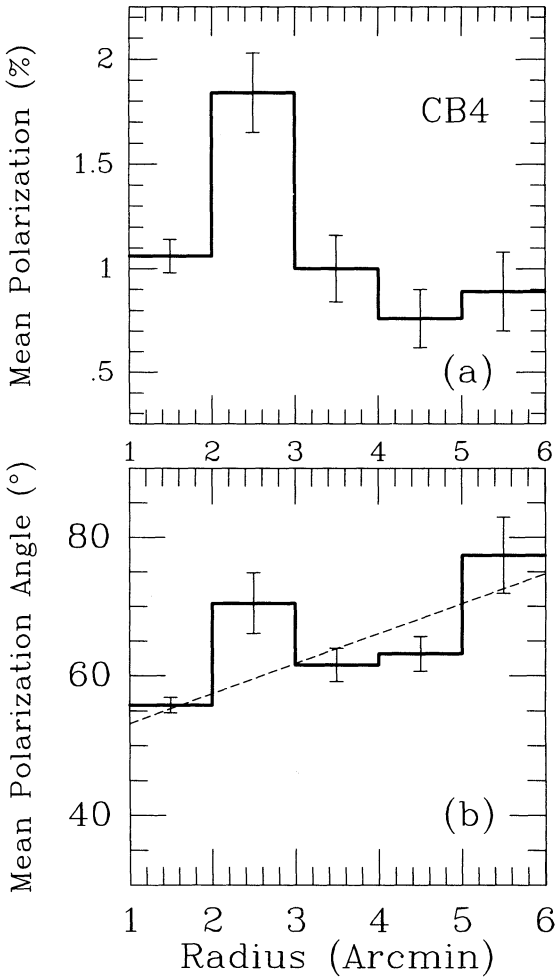

FIG. 9.—(*a*) Distribution of mean percentage polarization with radial separation from the center of CB 4. (*b*) Distribution of mean polarization position angle with radial separation from the center of CB 4. The dashed line represents the linear least-squares fit to the data.

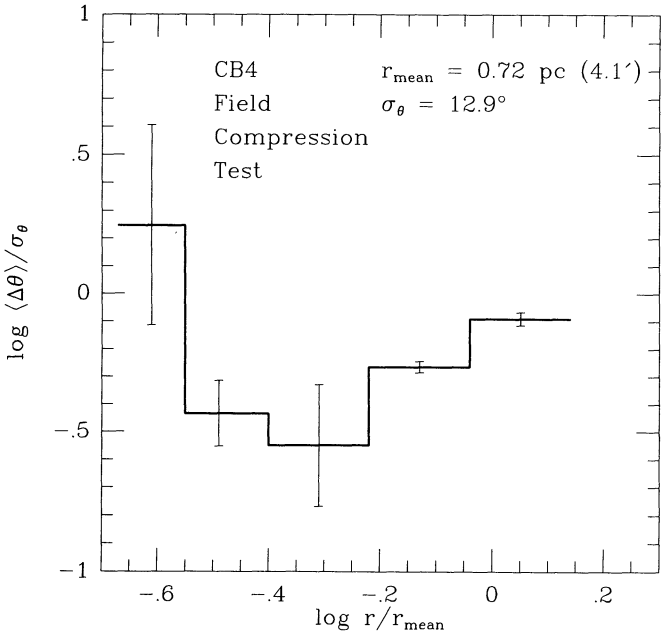

FIG. 10.—Distribution of normalized mean star-to-star differences of polarization position angle in CB 4, within normalized concentric bins of radius. Normalization factors are the angular dispersion of 12°.9 from Fig. 5, and the mean radius of 0.72 pc, which is the mean projected stellar distance from the center of the globule for the 80 stars in the polarization sample.

distances) mean polarization position angle and normalizing the average angular differences by the global position angle dispersion. In the case of no compression, the distribution would be essentially flat. In the case of strong compression, the distribution would contain a single maximum, at the characteristic radius where the degree of compression is greatest.

Figure 10 shows that at larger radii there is a rising trend, indicative of large-scale (greater than 1 pc) variations in the magnetic field direction. At smaller radii, the opposite rising trend may indicate field-line compression inward of 0.2 pc, ~1′. However, because of the opaque nature of the cloud core there is no polarimetric sampling of very small radii (less than 0.05 pc, ~18″). There appears to be no compression in the cloud periphery, and any core compression occurs too close to the globule center to be measured via optical polarimetry.

4.2.2. *Field Wrapping*

If there is significant coupling of ions and neutrons in a gas containing significant angular momentum, wrapping of field lines is expected. The presence of field wrapping was sought by comparing the azimuthal (Fig. 11) and radial (Fig. 9) distributions of mean polarization position angles.

Figures 11*a* and 11*b* demonstrate azimuthal variations of weighted mean polarization percentage and position angle. In the case of strong field wrapping, the azimuthal distribution in Figure 11*b* would be characterized by a broad peak, with small (less than 10°) dispersions in each bin. In the absence of field wrapping, the distribution would be flat with small dispersions in each bin. Comparing Figure 4 to the histogram in Figure 11*a*, it can be seen that there is a preponderance of high-polarization stars from P.A. = 45° to −135°, and a corresponding dearth of high-polarization stars from −135° to 45°. The high mean value region is denoted zone I in Figure 11, while the low mean value is denoted zone II.

This asymmetry is not an artifact of differing exposure times. Longer exposure times would produce on average more *low*-percentage polarizations in the southwest and northeast (see information about frames A and C in Fig. 1); the higher polarizations for stars in frames A and C rule out this possibility. The asymmetry may result from a real asymmetry in the dust distribution or from changes in the line-of-sight component of the magnetic field.

Figure 11*b* demonstrates the uniformity of weighted mean position angles (and thus of the magnetic field) in zone I. Dispersions of position angles in this zone are less than 5°. All mean position angles are within 1 σ (mean error) of each other and within 1 σ of the global mean of 63° (see Fig. 5). However, the distribution in zone II is noticeably different. Dispersions are larger ($\sigma > 10°$), and the mean position angles decrease smoothly with increasing azimuth. This type of variation, when taken in context with smaller polarizations, suggests that either the line-of-sight component of the magnetic field changes, or the ratio of nonuniform to uniform magnetic field strength changes, from zone I to zone II.

The zone I–to–zone II differences are best illustrated in Figure 12, which plots the weighted mean polarizations from

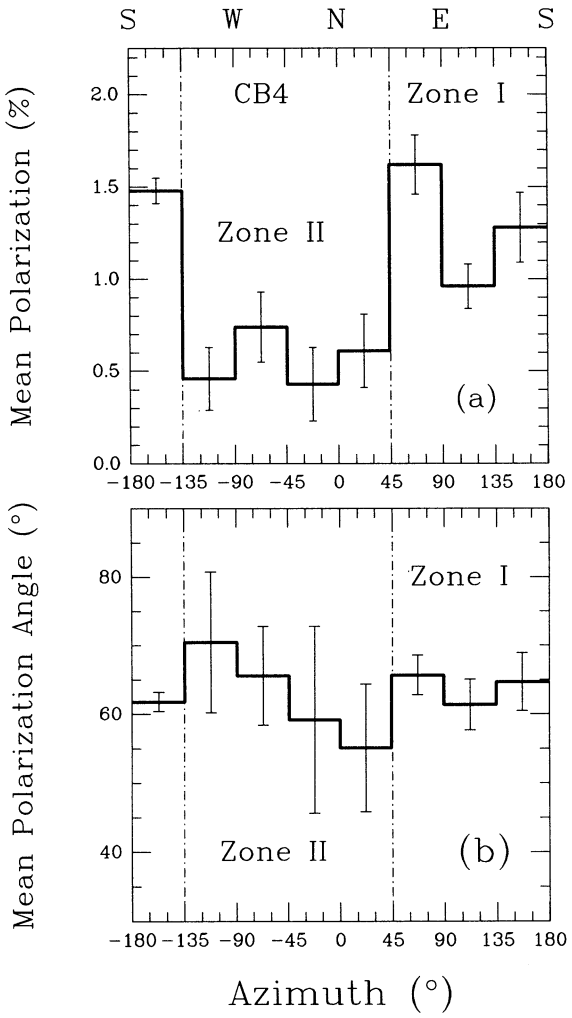

FIG. 11.—(*a*) Distribution of mean percentage polarization with bins of azimuth (position angle) relative to the center of CB 4. The distribution appears divided into two zones (zone I and zone II, see text). (*b*) Distribution of mean polarization position angle with bins of azimuth (position angle) relative to the center of CB 4.

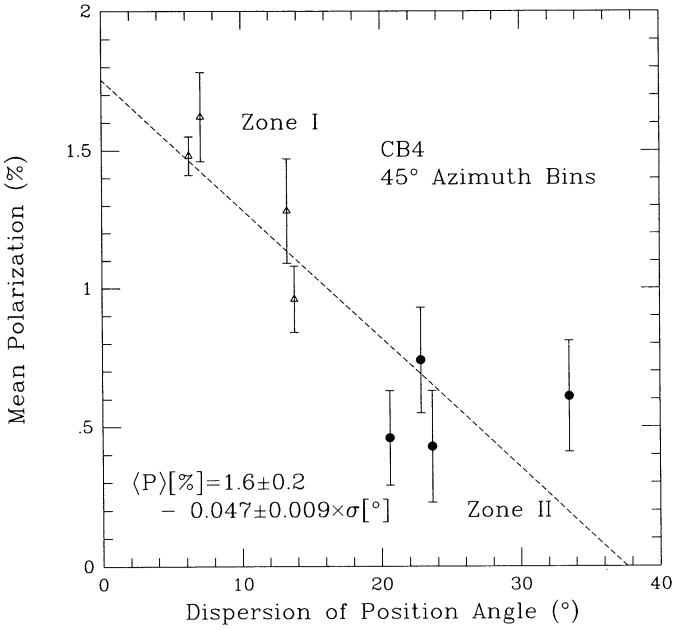

FIG. 12.—Distribution of weighted mean polarizations, binned in azimuth by 45°, as in Fig. 11, with the dispersion of polarization position angle. See description of zones I and II in text. The dashed line represents the least-squares fit to the data.

Figure 11*a* against the dispersion of the position angles from Figure 11*b*. The eight points represent the mean values computed for stars contained in 45° bins of azimuth. The dashed line is the best fit to the data and has a slope of −0.05% degree^{-1}. The correlation coefficient is −0.91, meaning that the mean polarization and the dispersion of the position angle are correlated with a likelihood exceeding 97%.

The azimuthal and radial symmetries of mean polarization position angles, taken together, indicate that there is no significant (less than 10° total) wrapping of field lines around CB 4, unlike the fields of many globules, whose cometary, or wrapped, field-line patterns (position angle changes up to 90°) suggest envelope interactions with energetic gas (Hodapp 1987). The uniformity of the field pattern of CB 4 effectively precludes fast rotation of an ionized envelope sweeping up frozen-in-field lines and wrapping them around the globule.

Observations of the positional variation in gas radial velocity constrain the cross-cloud velocity shift to be less than 0.07 km s^{-1} (DC), corresponding to a very slow rotation rate of less than 0.14 km s^{-1} pc^{-1} in the 0.5 pc envelope. New, high spectral resolution observations of CB 4 in ^{13}CO (Kane & Clemens 1995) show a maximum velocity gradient of less than 0.1 km s^{-1} pc^{-1}, along a direction perpendicular to the direction of both cloud elongation and the mean magnetic field. The magnitude of the velocity gradient is consistent with that expected from Galactic shearing forces, for a flat Galactic rotation curve; however, the direction is the opposite of that expected.

The ambipolar diffusion timescale, which depends only on the degree of ionization, is about one million years, for an ion fraction $x = 10^{-7}$ (Ciolek & Mouschovias 1993). The rotational timescale for CB 4, which depends only on the velocity gradient and radius, is a few tens of millions of years at a radius of 0.1 pc. Hence, these timescales are of the same order of magnitude only at very small radii (less than 10^{-2} pc, less than 2000 AU), which allows rapid diffusion of the field through the slowly rotating cloud envelope, preventing field-line wrapping.

In determining the ionization fraction it has been assumed that cosmic rays are the predominant source of ionization. If, instead, photoionization processes dominate in a clumpy globule medium (McKee 1989; Myers & Khersonsky 1995), the ionization fraction may be as high as $x = 10^{-6}$, leading to a longer ambipolar diffusion time.

4.2.3. *Position Angle Two-Point Correlation Function*

In the manner of Clemens, Dickman, & Ciardi (1992, hereafter CDC), the characterization of the variation of mean absolute-valued position angle differences for all star pairs with their plane-of-sky separations allows testing for an intrinsic magnetic field decorrelation length for the globule. This information is important in deducing the significance of the role played by a nonuniform magnetic field (including hydromagnetic wave phenomena) in the fragmentation of molecular clouds, or in the persistence of clumps. CDC found that the magnetic field decorrelation length and the mean ^{12}CO and

^{13}CO clump sizes in the CB 63 (LBN 11) globule were roughly the same (0.1–0.2 pc). For CB 4, there does not yet exist the high spatial and spectral resolution information needed to resolve small clumps of molecular material in the globule. Nevertheless, the magnetic field probe of CB 4 can be performed.

Figure 13*a* displays the two-point function of mean absolute-valued position angle difference with plane-of-sky separation, at the assumed CB 4 distance of 600 pc (DC), for zones I and II. To demonstrate the full range of separations, which span two orders of magnitude, the distances are binned and plotted logarithmically. The data have been oversampled by one-half bin. Figure 13*b* plots the two-point function for the sum of the two zonal data sets.

Figure 13 shows that the optical polarizations produce a weak peak at a distance logarithm of −1.1, similar to (but weaker than) that found by CDC for CB 63. This size scale is smaller than the CB 4 globule itself (as well as being smaller than the opaque core seen by DC) and cannot be identified with any scale length characteristic of the radial distributions of polarization and position angle (Figs. 9*a* and 9*b*). It may be due to the interaction of magnetic waves with clumps in the globule which are as yet unresolved. However, the decorrelation length for CB 4 is only mildly significant, and best seen in only one bin of separation. There is not much significant difference between the small-separation features in zones I and II.

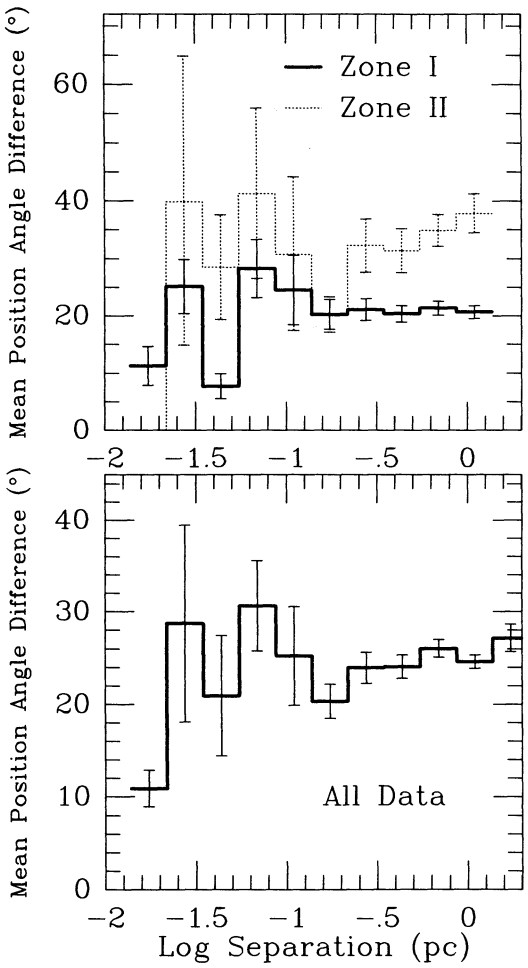

FIG. 13.—Distribution of binned, projected logarithmic separation between pairs of stars seen toward CB 4 vs. the mean of the absolute value of the difference in polarization angle for each star pair. The highest valued feature (at log separation of approximately −1) corresponds to an angular separation of 0.4, and a linear size of ~0.1 pc.

However, at larger separations (more than ~0.2 pc), the zone distributions are markedly different. In zone I, the mean position angle difference remains about 20°, while in zone II the mean position angle difference increases from more than 30° to almost 40°. Apparently, the nonuniform component of the magnetic field is more prominent in zone II than in zone I.

5. DISCUSSION

5.1. *The Magnetic Energy Budget*

From the somewhat smaller dispersion of the overall distribution of polarization position angles, the magnetic field around CB 4 appears to be more uniform and less perturbed than fields around star-forming dark clouds (MG). The smaller dispersion may be due to the smaller map size; the CB 4 map size is 9′, while MG maps typically cover a few degrees. The energetics of the uniform and nonuniform components of the magnetic field are quantifiable in several different ways, two of which are detailed below.

The ratio of nonuniform to uniform magnetic energy densities can be estimated, for a particular model of the field distribution consisting of a uniform field B with a nonuniform component represented as a Gaussian distribution of amplitudes, from equation (40) of MG:

$$\frac{M_n}{M_u} = \frac{DNs^2B_x^2}{B^2}, \tag{1}$$

where D is the number of dimensions in the field model (3), N is the number of field decorrelation lengths along the line of sight, s is the observed dispersion of the position angle distribution in radius, and B_x and B are the magnitudes of the uniform component of the plane-of-sky and total magnetic fields, respectively. For a uniform magnetic field, this magnetic field ratio $(B_x/B)^2$ averages to $\frac{1}{2}$. Since a possible field decorrelation length is found (§ 4.2.3) to be ~0.1 pc and the stellar photons are probably sampling ~0.5 pc (the envelope size) along the line of sight, N is likely to be ~5 for CB 4. The dispersion s in radians is 0.17, so the derived ratio M_n/M_u is 0.28. Hence, most of the energy density contained in the magnetic field around CB 4 appears to originate in its uniform component.

Another measure of the interaction of the magnetic field with gas and dust in the globule is the magnetic Reynolds number, the ratio of the ambipolar diffusion time to the sound crossing time:

$$R_{\rm mag} = \frac{\tau_{\rm ad}}{\tau_s}. \tag{2}$$

This ratio is

$$R_{\rm mag} = 0.24\left(\frac{x}{10^{-8}}\right)\left(\frac{T}{10\ {\rm K}}\right)^{1/2}\left(\frac{d}{0.12\ {\rm pc}}\right)^{-1}\left(\frac{\mu}{2m_{\rm H}}\right)^{-1/2}, \tag{3}$$

following Ciolek & Mouschovias (1993), where x is the ionization fraction, T the kinetic temperature, d the diameter of the globule core, and μ the mean molecular mass. A large ratio (more than 1) indicates that flux-freezing conditions dominate, whereas a small ratio indicates turbulent conditions dominate in the field. Using an enhanced value for the ionization fraction (10^{-7}), and the kinetic temperature (25 K) indicated by the

hot-edged polytrope models of DC for CB 4, the magnetic Reynolds number is only 1.1. The magnetic field around CB 4 indeed appears not to be strongly frozen into the gas and dust in the globule, as was argued earlier.

5.2. *The Nature and Location of Polarizing Grains*

As described in the discussion regarding Figure 9*a* in § 4.1, the polarization peaks toward the outer core of CB 4, favoring polarizing grains residing in the globule envelope. The interpretation for the decrease in polarization toward the center of the globule is not as certain, though. Often, dust grain destruction, or morphological and compositional variation of the grain, is invoked to explain central decreases in polarization (Leach et al. 1991, and references therein); in the case of CB 4 the former is highly unlikely, since the globule shows no signs of star formation (Clemens et al. 1991) and has a very optically opaque core ($A_v = 3$–5 mag; DC).

6. SUMMARY

The CCDPOL instrument has been demonstrated to be capable of obtaining detailed magnetic field direction maps toward small angular extent dark clouds. This CCD-based instrument has been used to probe the magnetic field pattern toward 80 stars around the small starless Bok globule CB 4. Analysis of this data set has established the following:

1. The magnetic field is very uniform in direction and apparently coupled to the Galactic field. The dispersion calculated from Gaussian fits of the polarization position angle distribution is only 10°, about one-third less than the mean dispersion for a sample of 15 dark clouds (MG). The ratio of uniform to nonuniform magnetic energy densities around CB 4 is ~ 4. The ratio of ambipolar diffusion time to sound crossing time is no more than unity, indicating little coupling of the magnetic field with the gas and dust associated with CB 4. The future evolution of CB 4 is likely field-free.
2. The mean polarization peaks about 2.5 (0.45 pc) from the globule core.
3. There is no indication of any significant wrapping of field lines around the globule. These results are consistent with CB 4 being a very slowly rotating globule in whose envelope the field slips easily. The ambipolar diffusion timescale is at least an order of magnitude smaller than the rotational period of the 0.1 pc core.
4. There is some indication of a magnetic field decorrelation length of ~ 0.1 pc, which is smaller than the visually opaque core. High-resolution submillimeter spectroscopy of the dense core of CB 4 may help to distinguish whether CB 4 contains stable clumps or transient phenomena.

This research was supported by NSF grant AST 92-21194 to D. C. We kindly thank Alyssa Goodman for comments and suggestions.

REFERENCES

Arquilla, R., & Goldsmith, P. F. 1986, ApJ, 303, 356
Barvainis, R. 1984, Ph.D. thesis, Univ. Massachusetts, Amherst
Blandford, R. D., & Payne, D. G. 1982, MNRAS, 199, 883
Ciolek, G. E., & Mouschovias, T. C. 1993, ApJ, 418, 774
Clemens, D. P., & Barvainis, R. 1988, ApJS, 68, 257 (CB)
Clemens, D. P., Dickman, R. L., & Ciardi, D. R. 1992, AJ, 104, 2165 (CDC)
Clemens, D. P., & Leach, R. W. 1987, Opt. Eng., 29, 923
Clemens, D. P., & Tapia, S. 1990, PASP, 102, 179
Clemens, D. P., Yun, J. L., & Heyer, M. H. 1991, ApJS, 75, 877
Dickman, R. L., & Clemens, D. P. 1983, ApJ, 271, 143 (DC)
Goodman, A. A., Bastien, P., Myers, P. C., & Ménard, F. 1990, ApJ, 359, 363
Goodman, A. A., Crutcher, R. M., Heiles, C., Myers, P. C., & Troland, T. H. 1989, ApJ, 338, L61
Hall, J. 1958, Publ. US Naval Obs., 2d Ser., 17, VI
Hodapp, K.-W. 1987, ApJ, 319, 842
Jones, T. J. 1989, ApJ, 346, 728
Joshi, U. C., Kulkarni, P. V., Bhatt, H. C., Kulshrestha, A. K., & Deshpande, M. R. 1985, MNRAS, 215, 275
Kane, B. D., & Clemens, D. P. 1995, in preparation
Kane, B. D., Clemens, D. P., & Myers, P. C. 1994, ApJ, 433, L49
Klebe, D., & Jones, T. J. 1990, AJ, 99, 638
Königl, A. 1989, ApJ, 342, 208
Leach, R. W., Clemens, D. P., Kane, B. D., & Barvainis, R. 1991, ApJ, 370, 257
Leung, C. M., Kutner, M. L., & Mead, K. N. 1982, ApJ, 262, 583
Martin, R., & Barrett, A. H. 1978, ApJS, 36, 1
Mathewson, D. S., & Ford, V. L. 1970, MmRAS, 74, 139
McKee, C. F. 1989, ApJ, 345, 782
Mouschovias, T. C., & Paleologou, E. V. 1980, ApJ, 237, 877
Myers, P. C., & Goodman, A. A. 1991, ApJ, 373, 509 (MG)
Myers, P. C., & Khersonsky, V. K. 1995, ApJ, 442, 186
Shu, F. H., Adams, F. C., & Lizano, S. 1987, ARA&A, 25, 23
Vrba, F. J., Luginbuhl, C. B., Strom, S. E., Strom, K. M., & Heyer, M. H. 1986, AJ, 92, 633
Yun, J. L. 1993, Ph.D. thesis, Boston Univ.
Yun, J. L., & Clemens, D. P. 1990, ApJ, 365, L73
Zaritsky, D., Shaya, E. J., Scoville, N. Z., Sargent, A. I., & Tytler, D. 1987, AJ, 93, 1514